Fusion Engineering and Design 224 (2026) 115612

Contents lists available at ScienceDirect

Fusion Engineering and Design

journal homepage: www.elsevier.com/locate/fusengdes

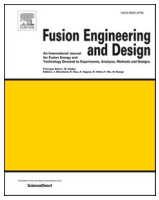

Thermal stability of tungsten fiber-reinforced tungsten composites fabricated by powder metallurgy

Svitlana Rudchenko [a,*], Yiran Mao [b], Wolfgang Pantleon [a]

[a] Technical University of Denmark, Department of Civil and Mechanical Engineering, Produktionstorvet 425, Kongens Lyngby, 2800, Denmark
[b] Forschungszentrum Jülich GmbH, Institute of Fusion Energy and Nuclear Waste Management, Wilhelm-Johnen-Straße, Jülich, 52425, Germany

ARTICLE INFO

Keywords:
Fusion materials
Plasma-facing components
Tungsten composite
Microstructural characterization
Thermal stability

ABSTRACT

Tungsten-based materials are considered as armor of plasma-facing components for future fusion reactors. To mitigate the brittleness of tungsten, tungsten fiber-reinforced tungsten composites (W_f/W) have been developed. Two types of W_f/W composites, with either continuous, aligned, potassium-doped tungsten wires in a dense tungsten matrix or randomly oriented, short fibers in a porous tungsten matrix are investigated. Both were fabricated using a powder metallurgical route facilitating field assisted sintering technology (FAST). Specimens are annealed at 1450 °C for different amounts of time up to two weeks to assess the thermal stability of the composites. Scanning electron microscopy and electron backscatter diffraction reveal major changes in the microstructure. After 4 hours of annealing initiation of recrystallization in the fibers concurrent to grain growth in the matrix is observed in both composites. Recrystallization commences at the outskirts of the fibers causing formation of a rim of small, recrystallized grains. Longer annealing increases the rim of recrystallized grains inwards into the fiber. After 3 days of annealing, all fibers are completely recrystallized, and the matrix is coarsened significantly by grain growth. While the short fibers can still be identified in the porous matrix after one week of annealing, matrix and continuous fibers cannot be distinguished any longer in the dense matrix. Short fibers with large, recrystallized grains can still be recognized after 2 weeks of annealing, while the porous matrix disintegrates by particle coarsening.

1. Introduction

Tungsten (W) and tungsten-based materials are the remaining candidate materials for the armor of plasma-facing components for future fusion reactors as ITER [1] or DEMO [2]. The armor materials to be used for plasma-facing components encounter different challenges from the high heat loads (stationary and transient) and particle fluxes causing degradation of mechanical properties and embrittlement by microstructural changes, hydrogen absorption or erosion.

Outstanding properties, including the highest melting point, high thermal conductivity, low propensity to recrystallization and strength at elevated temperatures, qualify tungsten as base material for components facing the burning plasma. Additionally, tungsten's resilience against erosion, good creep strength, low tritium retention, and relatively benign behavior under neutron irradiation further enhance its suitability, especially for the armor of plasma-facing components like the first wall and the divertor of fusion reactors [3,4]. The brittleness of tungsten reinstated under heat loads and neutron irradiation [5,6], however, remains a critical challenge for operation under high heat fluxes. Thermally activated restoration processes occur in the armor of plasma-facing components at their operation temperatures of 800 °C and above, for instance, in conventionally manufactured rolled tungsten plates [7,8]. The microstructural changes induced by recrystallization and grain growth embrittle tungsten-based components and enable crack initiation and rapid crack propagation during thermal cycling [9].

To overcome this drawback and to improve the damage resilience of tungsten, tungsten fiber-reinforced tungsten (W_f/W) composites consisting of drawn, potassium-doped tungsten wires as fibers (W_f) in a brittle tungsten matrix (W) are developed. W_f/W composites exhibit pseudo-ductile behavior at room temperature due to extrinsic toughening mechanisms during deformation and crack propagation. Plastic deformation of the fibers, fiber pullout, and interfacial debonding dissipate energy; additionally, crack deflections are caused by the fibers [10–12]. Drawn potassium-doped wires are used as fibers in fabricating of W_f/W composites due to their beneficial properties as high tensile strength and ductility at room temperature [13–15]. The improved

* Corresponding author.
E-mail address: sviru@dtu.dk (S. Rudchenko).

https://doi.org/10.1016/j.fusengdes.2025.115612
Received 20 October 2025; Received in revised form 10 December 2025; Accepted 31 December 2025
Available online 9 January 2026

damage resilience of W_f/W does not only rely on the ductility of the fibers but also on the interaction between fibers and matrix, for which weak bonding between both is crucial.

W_f/W composites can be manufactured by two different routes either by chemical vapor deposition (CVD) or by powder metallurgy (PM). CVD has been efficiently used for producing W_f/W composites with continuous fibers for many years [10,16], but despite the high reproducibility of the method, the production process is quite complex, time consuming and costly in terms of resources. Compared with CVD, the powder metallurgical production route has several benefits, such as existing experience with upscaling and bulk production, a higher production rate and the possibility of using tungsten alloys as matrix material [17–19]. However, it is crucial to consider that high temperatures during powder sintering can initiate restoration processes in the drawn wires. Originally, they were expected to have sufficient stability at high temperatures [15], but this was concluded from annealing for short times only [20] and their behavior during long-term annealing has not been investigated yet. Additionally, the wires may deform plastically, if the pressure during sintering is not applied hydrostatically. Hence, microstructural changes might be induced at high temperatures, lowering the ductility of the fibers. To mitigate the impact of temperature during sintering, field-assisted sintering technology (FAST) with only short sintering durations can be used [12,17].

Earlier studies of the thermal stability of a model composite produced by CVD and containing a single fiber [21–23] have shown that substantial restoration processes occur at high temperatures of 1400 °C and 1450 °C: recrystallization in the fiber and abnormal grain growth in the matrix, and subsequently, intergrowth between fiber and matrix. These restoration processes affect the mechanical properties significantly as shown for a multi-fiber composite [24]. Meanwhile, W_f/W composites fabricated via powder metallurgy have not yet been qualified as plasma-facing materials in terms of thermal stability.

In the present work, the thermal stability of powder metallurgically produced W_f/W composites is investigated considering their potential use as armor of plasma-facing components; two rather different types of composites are studied, containing either continuous, aligned tungsten fibers in a dense tungsten matrix or short, randomly ordered tungsten fibers in a porous tungsten matrix, respectively. To assess their thermal stability, high temperature annealing at 1450 °C for different durations up to two weeks is conducted. Such a temperature of 1450 °C exceeds the quasi-stationary operational temperature anticipated for the plasma-facing armor of a divertor in a fusion reactor and is expected to occur only intermittently. The high temperature is chosen here to accelerate the microstructural evolution and the associated restoration processes, enabling their observation over shorter, still rather long annealing times. The restoration processes and microstructural evolution in the fibers and matrix of the two different composites are characterized using scanning electron microscopy (SEM) and electron backscatter diffraction (EBSD).

2. Material and methods

2.1. Material

Two types of W_f/W composites, with either continuous, aligned tungsten fibers in a dense matrix (composite CD) or randomly oriented, short fibers in a porous matrix (composite SP) are fabricated by field assisted sintering technology (FAST), cf. Table 1. Pure tungsten powders with 5 μm average particle size and tungsten wires with diameter of 150 μm produced by OSRAM GmbH, were used as raw materials. The tungsten wires doped with 75 ppm potassium had elongated grains from wire drawing.

For manufacturing of composite CD, with aligned fibers in a dense matrix, fiber weaves are produced from tungsten wires with a distance of about 0.2 mm between parallel warp fibers and comparably large distances between the weft fibers. An yttria layer about 3 μm thick is deposited on the weaves by magnetron sputtering as interlayer separating fibers and matrix. Due to geometrical shadowing, this process has to be performed separately for each side of the weave. Tungsten weaves and tungsten powder were alternately put layer-by-layer into a graphite mold where all weaves are aligned with the warp fibers along the same direction. The layered arrangement is consolidated via FAST with a heating rate of 50 K min^{-1} and a holding time of 5 min at 1800 °C under a pressure of 50 MPa, for manufacturing details see [18].

For manufacturing of composite SP with short fibers in a porous matrix, pure tungsten powder and short tungsten fibers with 2.4 mm length were used. Tungsten fibers and powder are mixed by manual shaking in a vessel with a mass fraction of fibers of about 40 %. The mixture is evenly distributed into a graphite mold and consolidated by FAST with a heating rate of 100 K min^{-1} and a holding time of 4 min at 1400 °C under 60 MPa, for manufacturing details see [19].

As result, coin-shaped samples (with diameter of 40 mm and a height of about 5 mm) are produced. Subsequently, bars with a size of about 27 × 4 × 3 mm^3 are cut from the coin-shaped specimens (cf. Fig. 1). Before assessing the thermal stability of the composites, three-point bending tests were performed to investigate their fracture behavior with bending to failure for composite CD and only slight bending for composite SP [18,19].

2.2. Experimental procedure

The obtained bars of composites CD and SP are cut along their longest extension into smaller pieces about 4 × 3 × 0.5 mm^3 with plane-parallel surfaces using an Accutom-50 from Struers. The specimens are encapsulated in a quartz glass ampule to prevent oxidation during annealing, with each ampule containing one specimen of each type. The ampules are evacuated, flushed with argon, and evacuated again before sealing. Annealing at 1450 °C is carried out in a tube furnace Nabertherm RHTH 50-150/18. The furnace is pre-heated before the ampules are placed inside. After annealing for the desired time up to 2 weeks, the ampules with the specimens inside are removed from the furnace and opened after air-cooling to room temperature. Different specimens are used for each annealing time.

For microstructural characterization, one of the surfaces of each specimen (corresponding to cross sections of the original bars) is ground with SiC paper up to 4000 grit size, polished with a 3 μm and 1 μm diamond suspension and electropolished for approximately 5 s to 7 s in an aqueous solution containing 3 wt.% NaOH at room temperature. Electropolishing is performed with a voltage of 12 V and a current of 1.5 A. Cross-sectional views of the fiber composites CD and SP in their as-received state are shown in Fig. 2. Fiber and matrix can be clearly distinguished for both. The parallel alignment of the fibers in composite CD and the porous matrix of composite SR are also revealed. Orientation data are collected on the prepared surface using a Zeiss Sigma SEM equipped with a Cnano EBSD detector from Oxford instruments with an accelerating voltage of 20 kV. Acquisition is performed on square grids with different step sizes (1 μm or 0.5 μm) depending on the size of the area to be analyzed and the purpose of the acquisition. The data are

Table 1
Overview of the two types of W_f/W composites investigated.

Composite designation	Fibers	Arrangement	Matrix	Condition	Relative density	
CD	Continuous	Aligned	Dense	Deformed to failure	91 %	[18]
SP	Short	random	Porous	Slightly deformed	77 %	[19]

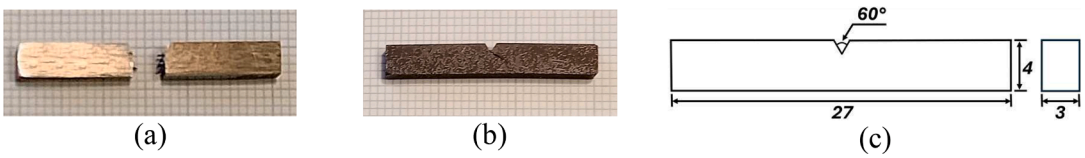

Fig. 1. Powder metallurgically fabricated multi-fiber tungsten fiber-reinforced tungsten composites in their as-received state (on millimeter paper): (a) composite CD with continuous, aligned tungsten fibers in a dense matrix, (b) composite SP with randomly oriented, short fibers in a porous matrix. (c) Sketch of the geometry with sizes in mm.

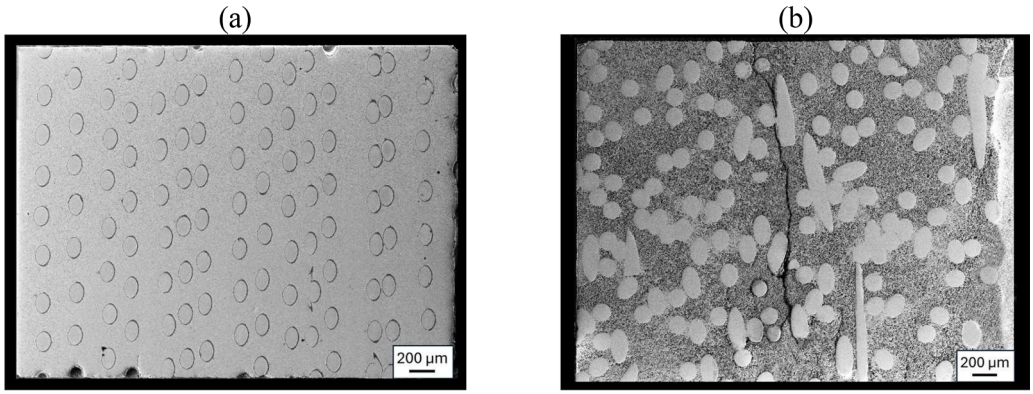

Fig. 2. Multi-fiber tungsten fiber-reinforced tungsten composites fabricated by powder metallurgy. Macroscopic overview of as-received states: (a) composite CD with continuous, aligned tungsten fibers in a dense matrix, (b) composite SP with randomly oriented, short fibers in a porous matrix. Secondary electron images obtained by SEM on cross sections.

analyzed using the Matlab plugin toolbox MTEX Version 5.11.2 [25]. All orientation maps are presented and analyzed without applying any filtering or removing non-indexed points. High angle boundaries (HABs) with disorientation angles above 15° are indicated in black, low angle boundaries (LABs) with disorientation angles above 2° but not exceeding 15° in white. Grains are identified as contiguous regions separated from others by HABs. For each grain the equivalent circular diameter is determined. Their area-weighted average value is determined excluding grains consisting of less than four pixels; the reported standard deviation of their distributions characterizes the width of the distribution not the accuracy of the average.

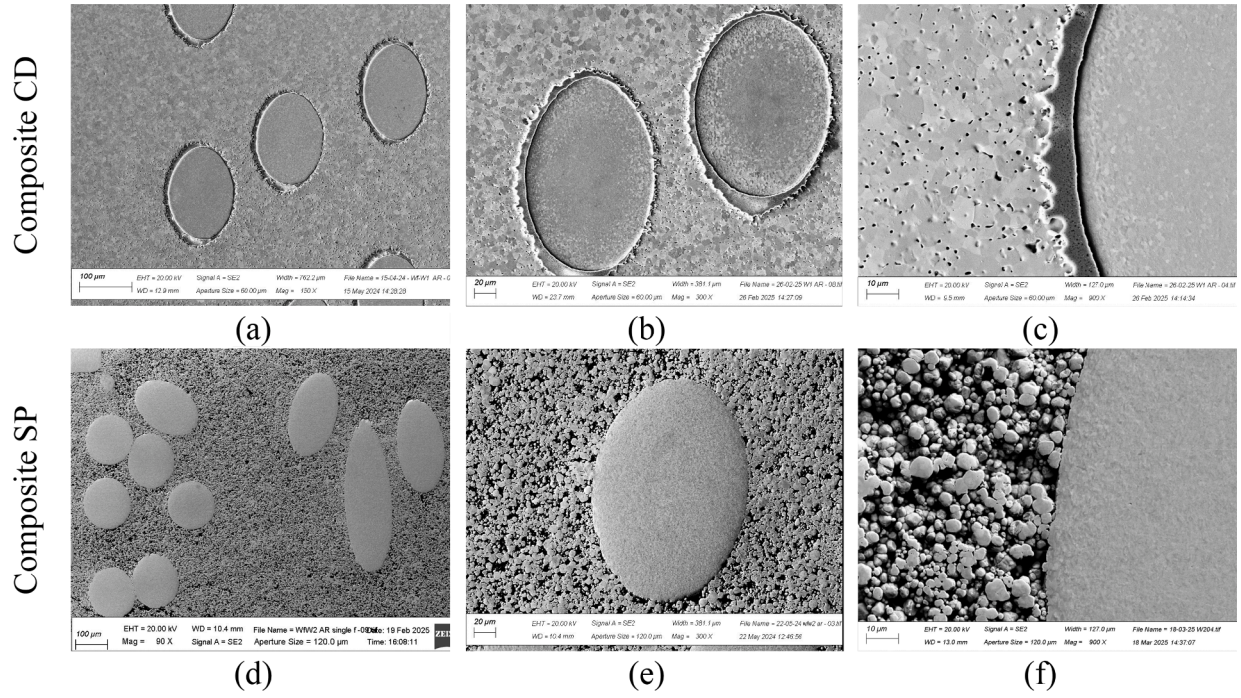

Fig. 3. Multi-fiber tungsten fiber-reinforced tungsten composites fabricated by powder metallurgy. Secondary electron images on cross sections obtained by SEM on the as-received composites with different magnification: (a,b,c) composite CD with interlayer of Y_2O_3 and (d,e,f) composite SP without any interlayer. While (a,b,d,e) give an overview of the microstructure, focus is on the interface between fiber and matrix in (c,f).

3. Results and discussion

3.1. As-received state

The microstructure of multi-fiber composites CD and SP in their as-received condition is presented in Fig. 3, where secondary electron images (from SEM) of cross sections of the composite CD with an yttria interlayer (Fig. 3a, b) and composite SP without any interlayer (Fig. 3d, e) are shown. In both cases, the drawn tungsten fibers and the tungsten matrix can be clearly distinguished from each other. Individual tungsten grains in the dense and the porous matrix are readily observed (Fig. 3a, b), while in the fibers, grains cannot be resolved individually in secondary electron images even with higher magnification (as shown in Fig. 3c, f). During wire drawing, the grains in the wire become elongated along the drawing direction with only a small cross section perpendicular to it [13].

For the composite CD, 15 fiber weaves were arranged layer-by-layer alternatingly with tungsten powder resulting in an average spacing between two weaves of 0.25 mm. Since weaves and powder were assembled manually in the mold [17], orientation and spacing of the fiber weaves are not perfectly uniform, as can be seen from Fig. 2a and Fig. 3a. All fibers in the as-received condition of composite CD show an elliptical shape in the cross section with same alignment and same aspect ratio of 1.6 throughout the entire cross section. Their cross-sectional area of about 17700 μm^2 still corresponds to that of the initial wires with diameter of 150 μm (with their major axis now larger and their minor axis smaller than 150 μm). As all fibers are aligned with the normal direction of the cross section and viewed edge-on, their observed ellipticity cannot be a projection effect (as confirmed by the maintained cross-sectional area) but must have been caused by plastic deformation during manufacturing or the subsequent bending test. As the latter introduces different strains throughout the cross section of the specimen, the main reason for the uniform elliptical shape is seen in the manufacturing process, most likely a non-hydrostatic pressure being applied during FAST – causing the same equivalent strain of 0.27 for all fibers, as determined from the aspect ratio of 1.6 assuming deformation under plane strain conditions.

In Fig. 3b, the yttria layer between fibers and matrix is clearly seen (appearing bright), but also some detachment from the fiber in the lower left where the interlayer is located between powder particles, i.e. the detachment must have happened before sintering, e.g. during mixing. Fig. 3c even shows a gap between interlayer and fiber as well as a jagged appearance of the yttria interlayer on the matrix side caused by matrix particles penetrating the interlayer during sintering [26]. The microstructure of the matrix is rather homogeneous: different regions of the bulk matrix show the same grain structure with equiaxed grains and only minor porosity. Statistical analysis of the grain size based on orientation maps obtained by EBSD from the cross section of composite CD reveals that the area-weighted average grain size of the matrix is 7.0 ± 3.2 μm with a rather large spread in the distribution.

An overview of the microstructure of composite SP with short fibers (of mass fraction 40 %) in a porous matrix is shown in Fig. 3d and Fig. 3e. The interface between fiber and matrix is highlighted in the enlarged Fig. 3f. Obviously, the porosity of the composite SP is significantly higher than that of composite CD (as intended) due to a lower sintering temperature of 1400 °C compared to 1800 °C for composite CD. It is observed from Fig. 3f that only a loose bonding between fiber and matrix is established. The different elliptical shapes of the fibers in the as-received state of composite SP in Fig. 2b and Fig. 3d are of pure geometrical origin; individual fibers are cut under random inclination angles in the cross section. The fibers show quite different cross-sectional areas, but the minor axis of the ellipses is always 150 μm indicating that no plastic deformation of the fibers has occurred (a potential non-hydrostatic load is mitigated by the porous matrix). The fiber with the most elongated shape on the right-hand side of Fig. 3d, for instance, is inclined by 72° towards the normal direction of the cross section. Analysis of the grain size in the cross section of composite SP by EBSD reveals that average grain size in the porous matrix is 3.9 ± 1.9 μm.

A more detailed assessment of the microstructure of the fibers enclosed in the matrix is provided by orientation mapping using EBSD. Fig. 4 shows orientation maps of a cross section of an original potassium-doped wire used as initial fiber, and the composites CD and SP where mainly a single fiber is present with parts of the dense or porous matrix in its vicinity.

The orientation map (Fig. 4a) of the cross section of a drawn wire as used for fabrication shows a microstructure with very small grains within the wire, as expected after wire drawing and previously observed [16,22,27]. A qualitative analysis of the grain size revealed an average grain size of 1.0 ± 0.6 μm without variation throughout the wire cross section. The green color observed in the wire indicates a strong, preferential alignment of crystallographic ⟨110⟩ directions with the wire axis, confirming the formation of a ⟨110⟩ fiber texture typical for wire drawing of body centered cubic metals [28,29]. However, during the drawing process, plastic deformation as well as the stress state are heterogeneous throughout the entire cross section of the wire. Shear stresses from the contact with the drawing dies cause variations in microstructural features and in texture close to the wire surface, in particular. The texture is sharpest in the center but more disperse towards the rim of the wire (cf [29]). The orientation map in Fig. 4a indeed reveals (by the green color) alignment of crystallographic ⟨110⟩ directions with the cross section normal. A strong ⟨110⟩ fiber texture is present in the core of the wire, while grains with deviating colors (mainly red and yellow alongside green) are observed at the wire periphery revealing different crystallographic directions (from ⟨100⟩ to ⟨110⟩) along the wire axis.

Fig. 4b and Fig. 4c present orientation maps of the cross sections of single fibers (and their vicinity) in composite CD and SP, respectively. In both cases, different grains can be clearly distinguished in the matrix by their different color revealing different crystallographic directions along the normal to the cross section. This direction corresponds in both cases to the wire axis as care was taken to find a wire without inclination towards the surface normal in composite SP. This is evident from its circular shape in Fig. 4c and the 110 pole figure provided in Fig. 4d showing a strong 110 pole along the surface normal. From the orientation map of composite CD in Fig. 4b, the yttria interlayer between fiber and matrix can be identified by a ring of non-indexed points (in white). Meanwhile, plenty non-indexed points on the map for composite SP occur because of substantial porosity.

Some microstructural modifications are observed in the fibers compared to the drawn wire as increased average grain sizes of 2.4 ± 1.1 μm for composite CD and 1.8 ± 0.7 μm for composite SP. This indicates that the fibers have already undergone some restauration during FAST, yet the specific nature of the restauration process (extended recovery or recrystallization) is out of scope of the current investigation. For both composites, the strong ⟨110⟩ fiber texture in the core of the wire is preserved, as well as the deviations of crystallographic alignment in the fiber periphery.

3.2. Annealed condition

The microstructural stability of W_f/W composites during annealing at 1450 °C is systematically investigated using orientation maps based on EBSD acquisitions. The analysis focuses on changes in grain size, as well as the texture evolution in the tungsten fibers. Distinct differences between short-term (up to 24 hours) and long-term (up to 2 weeks) annealing treatments occurred such that the observations are discussed subsequently in the following two sections.

3.2.1. Microstructural changes during short-term annealing at 1450 °C

Orientation maps obtained for fibers and their neighborhood on cross sections of composite CD (with yttria interlayer) and composite SP (without any interlayer) after annealing at 1450 °C for 4 h, 8 h and 24 h

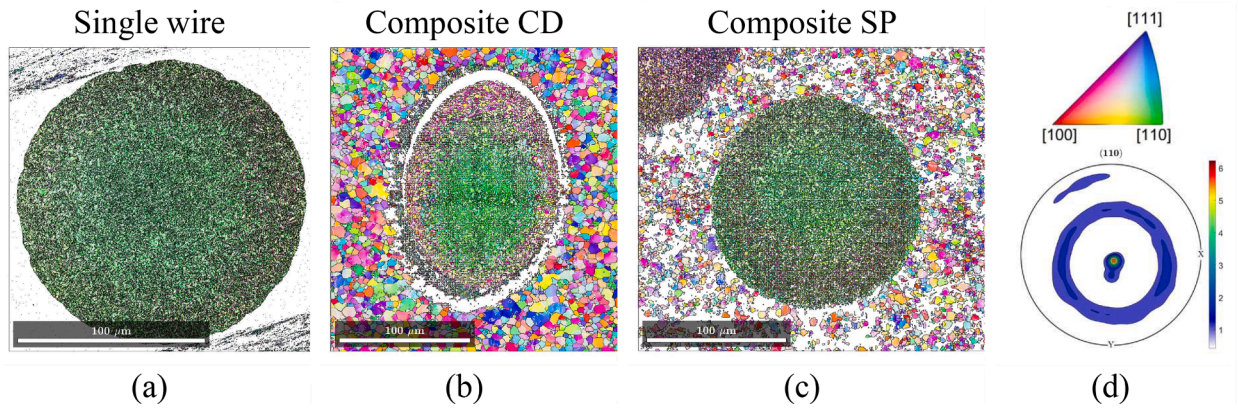

Fig. 4. Orientation maps obtained by EBSD on cross sections in the as-received state of (a) a potassium-doped tungsten wire, (b) a fiber in the dense matrix of composite CD and (c) a fiber in the porous matrix of composite SP. The maps are taken with the same magnification (300x) and step size 0.5 μm. The colors reflect the crystallographic directions along the direction normal to the cross section corresponding to the unit triangle shown in (d). This direction corresponds in all three cases to the wire axis. This is proven for the wire in composite SP by the 110 pole figure in (d) showing a strong 110 pole along the normal.

are collected in Fig. 5. The maps are shown with same magnification (as e.g. seen by the scale bars of equal length of 100 μm) to facilitate direct comparison of the microstructure of fibers and matrices between the as-received state and after annealing at 1450 °C for different durations.

The microstructures of both composites after short-term annealing at 1450 °C differ significantly from those in the as-received state, indicating ongoing restoration. For both composites, the fibers remain easily identifiable after annealing for up to 24 h. In case of composite CD with an yttria interlayer, the fibers are surrounded by a ring of non-indexed points appearing in white, indicating the presence of the interlayer and possibly opening gaps as well (Fig. 5a–c). In composite SP without interlayer between fiber and matrix (Fig. 5d–f), fibers can clearly be distinguished from the porous matrix by their different microstructures. The microstructure of the fibers evolves significantly, while the matrix remains porous with small, randomly oriented grains, its microstructure becomes harder and harder to resolve.

After 4 h of annealing of composite CD (Fig. 5a), recrystallization has clearly commenced close to the edge of the fiber and progresses inward. At the periphery of the fiber, the deformation structure is replaced by relatively large, equiaxed grains (15.5 ± 7.5 μm), forming a recrystallized rim. The recrystallized grains forming this rim display new orientations not belonging to the ⟨110⟩ fiber texture, which is dominantly present in the as-received state. In the core of the fiber, a central region still exists where the grains retain alignment of one of their ⟨110⟩ directions with the cross section normal. The grains in the fiber core appear of similar size (2.5 ± 1.4 μm) than those in the center of the fiber in the as-received state of composite CD (2.4 ± 1.1 μm). Grains in the surrounding dense matrix are larger than in the as-received state, indicating that grain growth occurred in the vicinity of the fiber already after 4 h of annealing at 1450 °C. The average grain size increased from

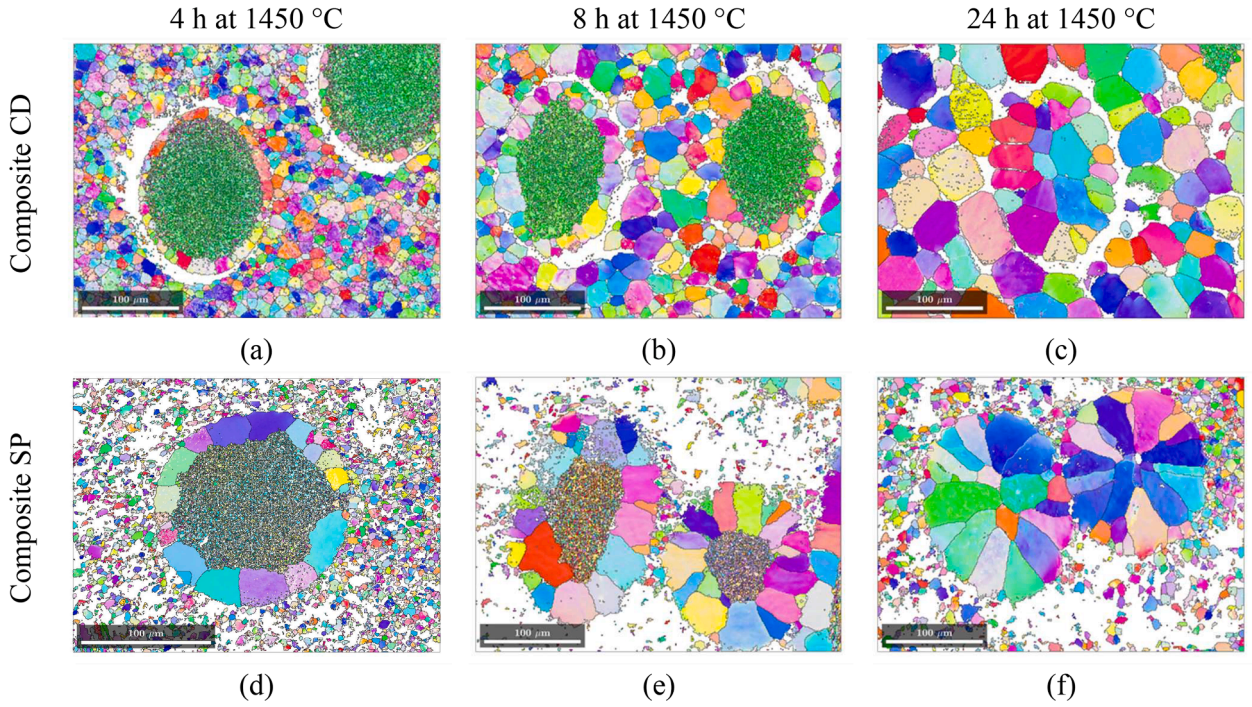

Fig. 5. Multi-fiber tungsten fiber-reinforced tungsten composites fabricated by powder metallurgy. Orientation maps of fibers and their vicinity obtained by EBSD with a step size of 1 μm on cross sections of composite CD with yttria interlayer (top row, a-c) and composite SP without interlayer (bottom row, d-f), after short-term annealing at 1450 °C for different durations: (a, d) 4 h, (b, e) 8 h, and (c,f) 24 h. The colors reflect the crystallographic directions along the direction normal to the cross section, as indicated by the unit triangle shown in Figure 4d.

7.0 ± 3.2 μm in the as-received state to 12.8 ± 5.3 μm during the first 4 h of annealing.

After 8 h of annealing at 1450°C, further growth of the recrystallized grains proceeds from the periphery inward into the fibers of composite CD. Grains with increased sizes of 23 ± 10 μm have developed in the matrix region, far exceeding those observed in the as-received state.

The microstructure evolution in the fibers of composite SP is quite similar to the one observed in composite CD, as shown in the orientation maps in Fig. 5d and Fig. 5e for 4 h and 8 h at 1450 °C, respectively. Recrystallization initiates close to the periphery of the fibers and progresses inward, accompanied by a gradual replacement of the deformation structure in the fiber cores with increasing annealing time. In contrast, the surrounding porous matrix exhibits only limited coarsening.

The microstructure of both composites changed substantially after 24 h of annealing at 1450°C as seen from Fig. 5c and Fig. 5f. The deformation structure within the fibers is no longer discernible. In composite CD, large, slightly elongated grains (with average size of 35 ± 11 μm) have replaced the original deformation structure indicating advancing recrystallization; the surrounding dense matrix exhibits further coarsening by grain growth to 39 ± 12 μm. The growth behavior in composite CD is summarized in Fig. 6. In the matrix, the square of the area-weighted average grain size evolves linearly with annealing time

$$d^2 = d_0^2 + kt \quad (1)$$

as expected for normal grain growth [30] with a growth coefficient k = 63 $\mu m^2/h$.

In contrast, composite SP shows a more limited response: while the microstructure in the fibers transforms by further growth of recrystallized grains of the rim towards the center, resulting in predominantly wedge-shaped grains (with average size of 46 ± 14 μm), the surrounding porous matrix displays only minor coarsening.

Comparison of the microstructures between composites CD and SP after 24 h of annealing at 1450 °C reveals significant differences in the progress of recrystallization within the fibers. While all fibers in composite SP appear fully recrystallized, composite CD still contains partially recrystallized fibers. Specifically, as concluded from the overview image of the entire cross section in Fig. 7a, 12 out of 112 fibers recrystallized only partially after 24 h. These randomly located, partially recrystallized fibers exhibit a microstructure similar to that observed after 8 hours of annealing: a rim of large, equiaxed grains surrounds a core composed of fine grains which still retains the alignment of one of their ⟨110⟩ directions. Moreover, these 12 fibers show different progress of recrystallized grains growing from the periphery inwards: the area of the core not overgrown by large grains varies from fiber to fiber, as illustrated by the three examples shown in Fig. 7b-d.

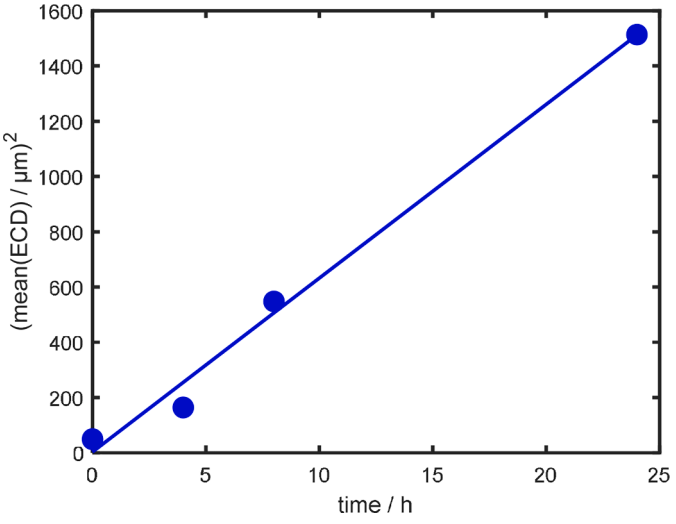

Fig. 6. Microstructure evolution of multi-fiber tungsten fiber-reinforced tungsten composite CD during annealing at 1450 °C up to 24 h: Evolution of area-weighted average grains size in the matrix.

It is important to note that single fiber model composites containing a single drawn tungsten fiber in a tungsten matrix produced by CVD do not show such a replacement of the microstructure in the fiber by large, recrystallized grains already after 1 day of annealing at 1450 °C, but only after 4 days [31]. This retarded behavior is observed for a 3 μm thick yttria interlayer as well as without any interlayer present and attributed to the lower processing temperatures during CVD compared to FAST.

3.2.2. *Microstructural changes during long-term annealing at 1450 °C*

The orientation maps obtained on cross sections of the composites after annealing at 1450 °C for more than 24 h and up to 2 weeks (Fig. 8) reveal continued microstructure evolution in both materials.

While the yttria interlayer in composite CD is clearly discernible in the as-received state and after short-term annealing, the interlayer is no longer evident after 3 days of annealing and beyond. The regions with non-indexed points surrounding the fibers (shown in white in Fig. 8a and Fig. 8b) correspond to voids formed as a result of morphological changes in the matrix during extensive grain growth. Such a disappearance of yttria from the interface between fibers and matrix has been observed earlier during sintering at high temperatures under different conditions [25] where some irregularly shaped yttria particles still were observed in between matrix grains.

After 3 days at 1450 °C, all fibers in composite CD are fully recrystallized and consist of a few large grains (with an average size of 44 ± 12 μm). These grains, distinguishable by their different colors indicating different orientations, formed during recrystallization of the fiber and subsequently underwent substantial growth. Despite the disappearance of the yttria interlayer, the original fiber locations remain distinguishable from the surrounding matrix, albeit less obvious than for shorter annealing durations. The matrix of composite CD coarsened significantly after 3 days of annealing, resulting in large, equiaxed grains with diameters of approximately 52 ± 17 μm. The overall impression of the microstructure in composite CD after 1 week of annealing at 1450 °C, displayed in Fig. 8b, is similar to that after 3 days of annealing, with continued grain growth observed in both the fibers and the matrix.

In contrast, after 2 weeks of annealing at 1450 °C the microstructure of composite CD changes entirely. As seen in Fig. 8c, fibers cannot be discerned from the matrix any longer. Tremendous grain growth has occurred in both fibers and matrix, rendering it impossible to distinguish between former fiber and matrix regions. The grains visible in the cross section are extremely large, with an average size of approximately 180 ± 64 μm, exceeding the original fiber diameter.

In case of composite SP, after 3 days or 1 week of annealing at 1450 °C (Fig. 8d and Fig. 8e), all fully recrystallized fibers exhibit some grain growth, along with coarsening of the matrix. After 2 weeks of annealing at 1450 °C, the short fibers and porous matrix in composite SP remain distinguishable (Fig. 8f). Each fiber contains only a few recrystallized grains, while the porous matrix becomes mechanically unstable and disintegrates under even minimal mechanical loads. Therefore, only a few grains are resolved at all in Fig. 8f.

4. Conclusions

Two types of powder-metallurgically produced tungsten fiber-reinforced tungsten composites were investigated: one with continuous, aligned fibers in a dense matrix (composite CD) and one with short, randomly oriented fibers in a porous matrix (composite SP). An yttria interlayer is present between fiber and matrix in composite CD, whereas in composite SP the fibers are embedded directly into the porous matrix. The thermal stability of the composites was characterized

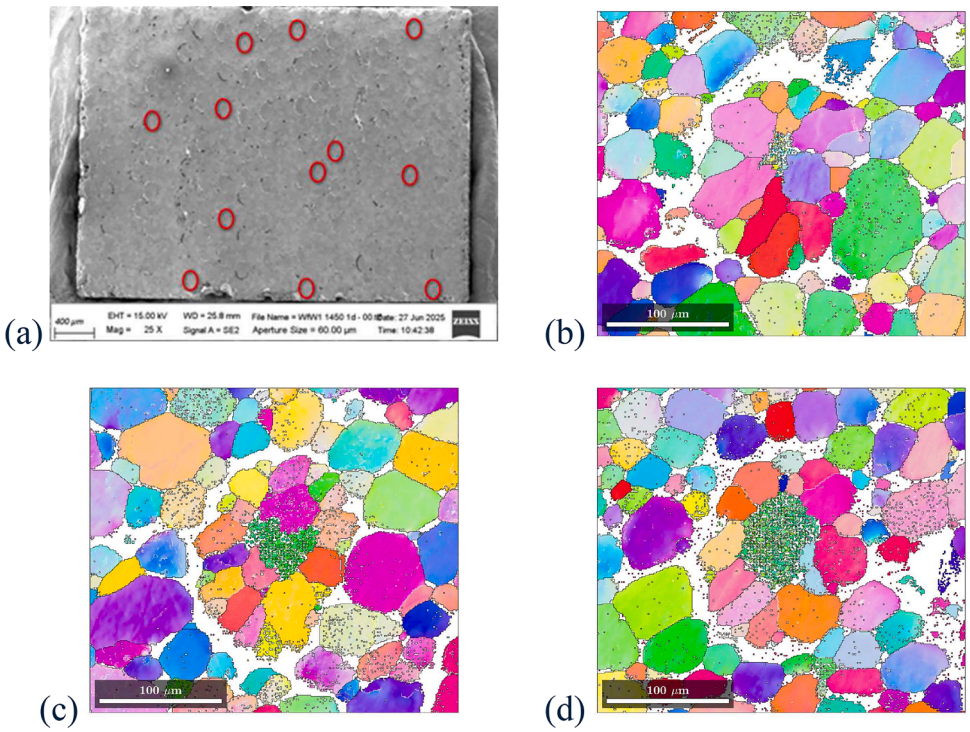

Fig. 7. Multi-fiber tungsten fiber-reinforced tungsten composite CD after annealing at 1450 °C for 24 h. (a) Secondary electron image obtained by SEM on entire cross section and (b,c,d) orientation maps of partially recrystallized fibers and their vicinity obtained by EBSD. The colors in the orientation maps reflect the crystallographic directions along the direction normal to the cross section, as indicated by the unit triangle shown in Figure 4d.

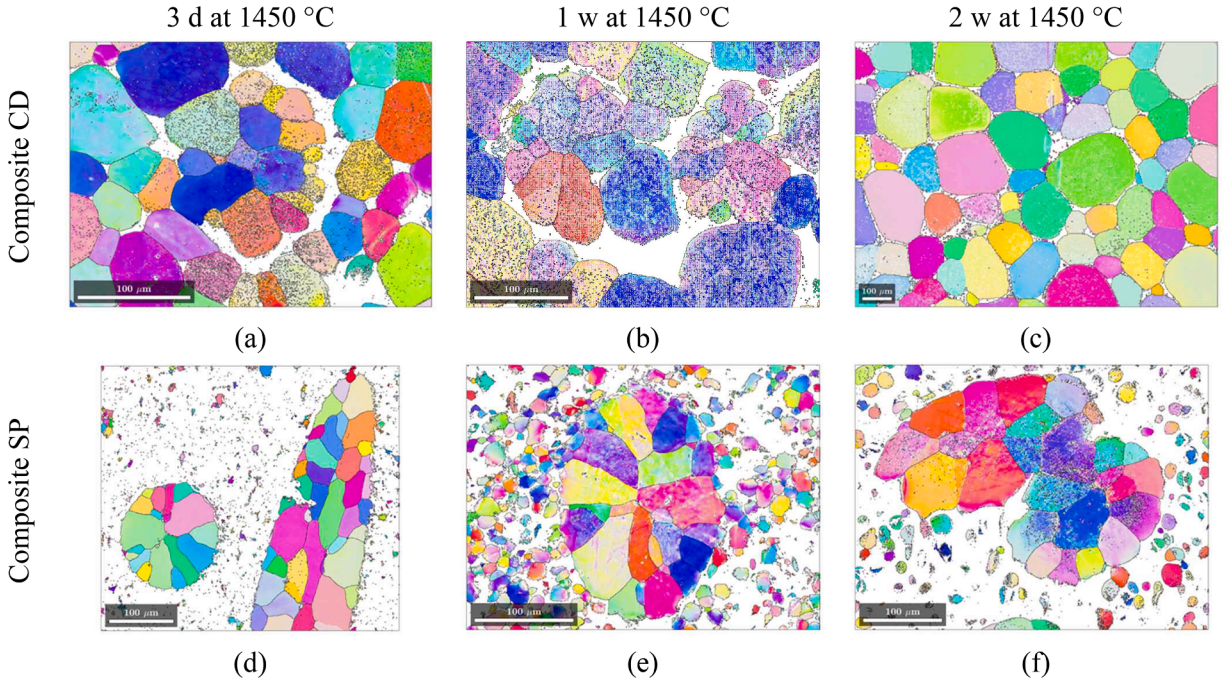

Fig. 8. Multi-fiber tungsten fiber-reinforced tungsten composites fabricated by powder metallurgy. Orientation maps of fibers and their vicinity obtained by EBSD with a step size of 1 µm on cross sections of composite CD with yttria interlayer (top row, a-c) and composite SP without interlayer (bottom row, d-f), after long-term annealing at 1450 °C for different durations: (a, d) 3 days, (b, e) 1 week, and (c, f) 2 weeks. The colors reflect the crystallographic directions along the direction normal to the cross section, as indicated by the unit triangle shown in Figure 4d.

by annealing at 1450 °C for durations up to two weeks.

For both composites, restoration processes initiate rapidly. After just 4 hours at 1450 °C, recrystallization of the tungsten fibers commenced at their periphery, forming rims of large, equiaxed grains, while the surrounding matrix undergoes noticeable grain growth. With increasing annealing time, recrystallization progresses inward and is completed after 1 day for all fibers in composite SP and the vast majority of fibers in composite CD. The dense matrix of composite CD undergoes extensive

grain growth, eventually coarsening beyond the original fiber size after two weeks. At this stage, individual fibers can no longer be distinguished from the matrix, indicating complete microstructural homogenization and loss of the original composite architecture.

In contrast, composite SP retains the distinction between fiber and porous matrix even after two weeks of annealing. Although the fibers are fully recrystallized and contain only a few large grains, they remain structurally separated from the porous matrix, while the porous matrix becomes mechanically unstable at this stage due to particle coarsening and loss of cohesion between particles.

These findings demonstrate that both types of W_f/W composites are microstructurally unstable at high temperatures. Full recrystallization of the fibers, intergrowth of the dense matrix and fibers, and disintegration of the porous matrix observed during prolonged exposure to a temperature exceeding the operating temperatures for plasma-facing components in the fusion reactors will lead to a loss of pseudo-ductility. After exposure of W_f/W composites to high temperatures, the expected extrinsic toughening mechanisms cannot persist, and subsequent failure of the component becomes likely. Therefore, their application as plasma-facing material should be limited to lower operation temperatures (e.g. not exceeding 1050 °C for an expected duration of 2 full power years), while overheating is permissible only for short time periods.

Data availability

Datasets related to this article will be made available through MATEDDI (Materials – Engineering Data and Design Integration).

CRediT authorship contribution statement

Svitlana Rudchenko: Writing – review & editing, Writing – original draft, Visualization, Validation, Methodology, Investigation, Formal analysis, Data curation. **Yiran Mao:** Writing – review & editing, Resources. **Wolfgang Pantleon:** Writing – review & editing, Writing – original draft, Supervision, Methodology, Funding acquisition, Conceptualization.

Declaration of competing interest

The authors declare that they have no known competing financial interests or personal relationships that could have appeared to influence the work reported in this paper.

Acknowledgements

This work has been carried out within the framework of the EUROfusion Consortium, funded by the European Union via the Euratom Research and Training Programme (Grant Agreement No 101052200 — EUROfusion). Views and opinions expressed are, however, those of the authors only and do not necessarily reflect those of the European Union or the European Commission. Neither the European Union nor the European Commission can be held responsible for them. Lars Lorentzen from DTU Risø campus is acknowledged for encapsulating.

Appendix. Thermal activated processes (cf. [7])

In general, the reaction rate of a thermally activated process follows an Arrhenius relation

$$\dot{\Gamma} = \nu \exp\left(-\frac{Q}{RT}\right)$$

with a jump frequency ν, the universal gas constant R, the absolute temperature T and an activation energy Q. If the process occurs unaltered, the reaction progress at different temperatures is additive and obtained for any time-dependent temperature history $T(t)$ by time integration

$$\Gamma = \int_{t_0}^{t} \nu \exp\left(-\frac{Q}{RT(t')}\right) dt'.$$

Assuming constant activation energy, the time t_1 to achieve a certain reaction progress at a temperature T_1, can be converted to a time

$$t_2 = t_1 \exp\left(\frac{Q}{R}\left(\frac{1}{T_2} - \frac{1}{T_1}\right)\right)$$

for which the same reaction progress is attained at another temperature T_2.

Table A1 provides the times t_2 predicted for achieving the same reaction process at a temperature T_2 as for a time t_1 of 24 h at a temperature T_1 of 1450 °C. As the activation energies for restoration in drawn potassium-doped tungsten wires are not known, two extreme activation energies 579 kJ/mol [32] and 352 kJ/mol [33] observed for the time to half recrystallization of tungsten plates rolled to different thickness reduction are considered. If the restoration processes occurring in W_f/W composites during 24 h annealing at 1450 °C must be avoided for their use as plasma-facing armor during 2 full power years of operation, the quasi-stationary operation temperature must be below 1100 °C to accommodate the worst scenario with lowest activation energy. Quasi-stationary operation temperatures not exceeding 1050 °C should be considered for using the investigated W_f/W composites as plasma-facing armor in view of intermittently occurring overheating events accelerating microstructural evolution [7].

Table A1
Estimated times t_2 for a thermal activation process occurring at certain temperatures T_2 achieving the same reaction progress as for a time t_1 of 24 h at a temperature T_1 of 1450 °C assuming two different activation energies.

Activation energy	1450 °C	1300 °C	1200 °C	1150 °C	1100 °C	1050 °C	1000 °C
579 kJ/mol	1 d	47 d	2.6 y	13.7 y	81 y	553 y	4371 y
352 kJ/mol	1 d	10.5 d	65 d	177 d	1.4 y	4.6 y	16.1 y

References

[1] R.A. Pitts, et al., A full tungsten divertor for ITER: Physics issues and design status, J. Nucl. Mater. 438 (2013) S48, https://doi.org/10.1016/j.jnucmat.2013.01.008.

[2] G. Pintsuk, et al., Materials for in-vessel components, Fusion Eng. Des. 174 (2022) 112994, https://doi.org/10.1016/j.fusengdes.2021.112994.

[3] V. Philipps, Tungsten as material for plasma-facing components in fusion devices, J. Nucl. Mater. 415 (1) (2011) S2–S9, https://doi.org/10.1016/j.jnucmat.2011.01.110.

[4] J.W. Coenen, S. Antusch, M. Aumann, W. Biel, J. Du, J. Engels, S. Heuer, A. Houben, T. Hoeschen, B. Jasper, et al., Materials for DEMO and reactor applications – boundary conditions and new concepts, Phys. Scr. T167 (2016) 014002, https://doi.org/10.1088/0031-8949/2016/T167/014002.

[5] G. Pintsuk, I. Bobin-Vastra, S. Constans, P. Gavila, M. Rödig, B. Riccardi, Qualification and post-mortem characterization of tungsten mock-ups exposed to cyclic high heat flux loading, Fusion Eng. Des. 88 (2013) 1858–1861, https://doi.org/10.1016/j.fusengdes.2013.05.091.

[6] H. Bolt, V. Barabash, G. Federici, J. Linke, A. Loarte, J. Roth, K. Sato, Plasma facing and high heat flux materials - needs for ITER and beyond, J. Nucl. Mater. 307–311 (1) (2002) 43–52, https://doi.org/10.1016/S0022-3115(02)01175-3.

[7] W. Pantleon, Thermal stability of the microstructure in rolled tungsten for fusion reactors, Phys. Scr. 96 (2021) 124036, https://doi.org/10.1088/1402-4896/ac2854.

[8] T. Larsen, K. Chmelar, B.L. Larsen, P. Nagy, K. Wang, W. Pantleon, Fusion Eng. Des. 192 (2023) 113581, https://doi.org/10.1016/j.fusengdes.2023.113581.

[9] T. Hirai, G. Pintsuk, M. Batilliot, Cracking failure study of ITER-reference tungsten grade under single pulse thermal shock loads at elevated temperatures, J. Nucl. Mater. 390-391 (2009) 751–754, https://doi.org/10.1016/j.jnucmat.2009.01.313.

[10] J. Riesch, M. Aumann, J.W. Coenen, H. Gietl, G. Holzner, T. Höschen, P. Huber, M. Li, C. Linsmeier, R. Neu, Chemically deposited tungsten fibre-reinforced tungsten – The way to a mock-up for divertor applications, Nucl. Mater. Energy. 9 (2016) 75–83, https://doi.org/10.1016/j.nme.2016.03.005.

[11] J. Riesch, J.Y. Buffiere, T. Höschen, M. Scheel, C. Linsmeier, JH. You, Crack bridging in as-fabricated and embrittled tungsten single fibre-reinforced tungsten composites shown by a novel in-situ high energy synchrotron tomography bending test, Nucl. Mater. Energy. 15 (2018) 1–12, https://doi.org/10.1016/j.nme.2018.03.007.

[12] R. Shu, Y. Mao, J.W. Coenen, A. Terra, S. Schönen, J. Riesch, C. Linsmeier, C. Broeckmann, Fabrication and fracture behaviors of the continuous brittle fiber reinforced tungsten composites fabricated via field-assisted sintering technology, Tungsten 7 (2025) 172–182, https://doi.org/10.1007/s42864-024-00291-z).

[13] P. Schade, 100 years of doped tungsten wire, Int. J. Refract. Met. Hard Mater. 28 (2010) 648–660, https://doi.org/10.1016/j.ijrmhm.2010.05.003.

[14] J. Riesch, J. Almanstötter, J.W. Coenen, M. Fuhr, H. Gietl, Y. Han, T. Höschen, C. Linsmeier, N. Travitzky, P. Zhao, Properties of drawn W wire used as high performance fibre in tungsten fibre-reinforced tungsten composite, Conf. Ser.: Mater. Sci. Eng. 139 (2016) 012043, https://doi.org/10.1088/1757-899X/139/1/012043.

[15] J. Riesch, Y. Han, J. Almanstötter, J.W. Coenen, T. Höschen, B. Jasper, P. Zhao, C. Linsmeier, R. Neu, Development of tungsten fibre-reinforced tungsten composites towards their use in DEMO—potassium doped tungsten wire, Phys. Scr. 2016 (T167) (2016) 014006, https://doi.org/10.1088/0031-8949/T167/1/014006.

[16] L. Raumann, J.W. Coenen, J. Riesch, Y. Mao, H. Gietl, T. Höschen, C. Linsmeier, O. Guillon, Modeling and validation of chemical vapor deposition of tungsten for tungsten fiber reinforced tungsten composites, Surf. Coating. Technol. 381 (2020) 124745, https://doi.org/10.1016/j.surfcoat.2019.06.065.

[17] Y. Mao, J.W. Coenen, C. Liu, A. Terra, X. Tan, J. Riesch, T. Höschen, Y. Wu, C. Broeckmann, C. Linsmeier, Powder Metallurgy Produced Aligned Long Tungsten Fiber Reinforced Tungsten Composites, J. Nucl. Eng. 3 (2022) 446–452, https://doi.org/10.3390/jne3040030.

[18] R. Shu, Y. Mao, A. Martinez-Pechero, J.W. Coenen, A. Terra, S. Schönen, J. Riesch, C. Linsmeier, C. Broeckmann, Study on the fracture behavior and toughening mechanisms of continuous fiber reinforced $W_f/Y_2O_3/W$ composites fabricated via powder metallurgy, Composites Part B 287 (2024) 111845, https://doi.org/10.1016/j.compositesb.2024.111845.

[19] Y. Mao, J.W. Coenen, S. Sistla, C. Liu, A. Terra, X. Tan, J. Riesch, T. Hoeschen, Y. Wu, C. Broeckmann, C. Linsmeier, Design of tungsten fiber-reinforced tungsten composites with porous matrix, Mater. Sci. Eng. A. 817 (2021) 141361, https://doi.org/10.1016/j.msea.2021.141361.

[20] V. Nikolić, J. Riesch, R. Pippan, The effect of heat treatments on pure and potassium doped drawn tungsten wires: Part I - Microstructural characterization, Mater. Sci. Eng. A. 737 (2018) 422–433, https://doi.org/10.1016/j.msea.2018.09.027.

[21] U.M. Ciucani, L. Haus, H. Gietl, J. Riesch, W. Pantleon, Microstructural evolution in single tungsten fiber-reinforced tungsten composites during annealing: recrystallization and abnormal grain growth, J. Nucl. Mater. 543 (2021) 152579, https://doi.org/10.1016/j.jnucmat.2020.152579.

[22] D.A.H. Wartacz, J. Riesch, K. Pantleon, W. Pantleon, Tungsten fiber-reinforced tungsten composites and their thermal stability, J. Nucl. Mater. 592 (2024) 154951, https://doi.org/10.1016/j.jnucmat.2024.154951.

[23] D.A.H. Wartacz, J. Riesch, K. Pantleon, W. Pantleon, Restoration in drawn tungsten wires of tungsten fiber-reinforced tungsten composites, Fus. Eng. Des. 216 (2025) 115038, https://doi.org/10.1016/j.fusengdes.2025.115038.

[24] D.A.H. Wartacz, T. Höschen, J. Riesch, K. Pantleon, W. Pantleon, Thermal stability of multi-fiber tungsten fiber-reinforced tungsten composites and their mechanical integrity after high temperature annealing, Fus. Eng. Des. 222 (2026) 115438, https://doi.org/10.1016/j.fusengdes.2025.115438.

[25] F. Bachmann, R. Hielscher, H. Schaeben, Texture Analysis with MTEX – Free and Open Source Software Toolbox, Solid State Phenom 160 (2010) 63–68, https://doi.org/10.4028/www.scientific.net/SSP.160.63.

[26] R. Shu, Y. Mao, J.W. Coenen, A. Terra, C. Liu, S. Schönen, T. Hoeschen, J. Riesch, C. Broeckmann, C. Linsmeier, Microstructure and mechanical properties of W_f/W composites influenced by Y_2O_3 coating, Int. J. Refract. Met. Hard Mat. 115 (2023) 106322, https://doi.org/10.1016/j.ijrmhm.2023.106322.

[27] M. Fuhr, J. Almanstötter, J. Riesch, R. Neu, W. Pantleon, Quantification of grain curling in drawn tungsten wires. In Preparation for Materials Characterization, 2026.

[28] W.F. Hosford, Microstructural Changes During Deformation of [011] Fiber-Textured Metals, Trans. Metall. Soc. AIME 230 (1964) 12–15.

[29] W. Pantleon, Fiber textures revisited, Mater. Char. 223 (2025) 114900, https://doi.org/10.1016/j.matchar.2025.114900.

[30] P.A. Beck, J.C. Kremer, L.J. Demer, M.L. Holzworth, Grain growth in high-purity aluminum and an aluminum-magnesium alloy, Trans. AIME 175 (1948) 372–400.

[31] D.A.H. Wartacz, J. Riesch, K. Pantleon, W. Pantleon, Recrystallization and grain growth in single tungsten fiber-reinforced tungsten composites, J. Phys.: Conf. Ser. 2635 (2023) 012034, https://doi.org/10.1088/1742-6596/2635/1/012034.

[32] A. Alfonso, D. Juul Jensen, G.-N. Luo, W. Pantleon, Recrystallization kinetics of warm-rolled tungsten in the temperature range 1150–1350 °C, J. Nucl. Mater. 455 (2014) 591–594, https://doi.org/10.1016/j.jnucmat.2014.08.037.

[33] A. Alfonso, D. Juul Jensen, G-N Luo, W. Pantleon, Thermal stability of a highly-deformed warm-rolled tungsten plate in the temperature range 1100–1250 °C, Fusion Eng. Des. 98-99 (2015) 1924–1928, https://doi.org/10.1016/j.fusengdes.2015.05.043.